Chapter 9
The Plasma Atom

Abstract In this chapter the statistical description of atomic radiative-collisional processes for complex heavy ions in electron atomic collisions is developed. The local plasma frequency model and the Thomas-Fermi electron density distribution are applied for the description of collisional processes making it possible to express the atomic characteristics (energy structure and oscillator strengths) as well as transition probabilities in terms of a functional of the electron density distribution inside atoms and ions. The Fermi method of equivalent photons allows to express the collisional rates in terms of photo-excitation or ionization cross sections. The statistical description is applied for efficient calculations of ionization cross sections and rates for different highly charged ions demonstrating a very good correspondence with detailed quantum mechanical calculations. Likewise, the dielectronic recombination rates obtained from statistical models are compared with quantum results for different ionization states of many chemical elements. The statistical method is in very good agreement with sophisticated detailed level-by-level quantum calculations and is of much higher precision than the usually applied Burgess formula. Finally, the statistical approach is applied for calculations of radiative energy losses of tungsten ions in hot thermonuclear plasmas. The results for the low-density case (coronal condition) of magnetically confined plasmas demonstrate a rather good correspondence with more detailed numerical calculations and measurements. In addition, the transition from the low-density corona condition to the high-density Boltzmann limit can be described via a simple application of detailed balance in the two-state approximation. In general, quite reasonable precision of the statistical model for different kinds of radiative-collisional processes is demonstrated. Moreover, general formulae and scaling relations can be obtained from the statistical approach that would otherwise difficult to obtain.

9.1 The Thomas–Fermi Statistical Approach

From the earliest days of quantum mechanics, it has been clear that one could not hope to solve exactly most of the physically interesting systems, especially those with three or more particles. This has stimulated the development of a large variety

F. B. Rosmej et al., *Plasma Atomic Physics*, Springer Series on Atomic, Optical, and Plasma Physics 104, https://doi.org/10.1007/978-3-030-05968-2_9

of approximate methods such as the time-dependent and time-independent perturbation theory, variational methods, and the Hartree method. The improvements of the Hartree method, namely the Hartree–Fock–Slater and the Dirac–Hartree–Fock–Slater (including the multiconfiguration Hartree–Fock (MCHF) method that incorporates configuration interaction and intermediate coupling, or its relativistic version MCDF—multiconfiguration Dirac–Fock method), are currently the most general and widely used methods to study the atomic structure of atoms and ions (Cowan 1981; Grant et al. 1980).

The theoretical description of multielectron systems and in particular the structure of heavy atoms and ions is still challenging, and one of the traditional approaches to this problem is the use of the Thomas–Fermi statistical theory (Fermi 1928; Gombas 1943, 1949, 1963; Lieb and Simon 1977; Kemister and Nordholm 1982). The Thomas–Fermi model represents the simplest way to take into account not only the Pauli principle, but also the mutual electrostatic repulsion of the electrons, at least in a general way, in a many-electron system. The starting point is the only approximately correct idea that there is a fixed potential well and that it is the same for all electrons. The model therefore gives a similar electron density for all atoms. Although the model does not permit to provide very detailed information about the atomic structure, it provides general insight into the properties of heavy atoms, e.g., the electron density distribution, ionization energies, size of the atom/ion, polarizability. The Thomas–Fermi model is also used to describe the equation of state of highly compressed and ionized matter, has stimulated the development of the density functional theory, and provides often a good starting point for more complex self-consistent field calculations.

Apart the atomic structure itself, the study of the interaction of multielectron atoms and ions with an electromagnetic field is of great practical interest due to applications in material science, atomic physics, plasma physics, radiative properties of matter, spectroscopy. The statistical model provides the possibility of a universal description of elementary processes (Astapenko et al. 2002, 2003) and radiative properties (Demura et al. 2013, 2015a, b) and to extract general scaling laws for all nuclear charges using the Thomas–Fermi density distribution $n(r)$. This is of particular interest for the fusion science: In magnetic fusion, high-Z divertor material (tungsten) is employed while in inertial fusion, high-Z materials (gold) are used as a hohlraum material. The determination of the detailed atomic structure (MCHF or MCDF) and corresponding radiative properties of these high-Z elements is, however, very challenging. Therefore, approximate and/or general methods are of great interest to derive the variety of requested properties. Moreover, more general methods and scaling relations are particularly useful for implementation of heavy element atomic physics in integrated simulations.

In the framework of the Thomas–Fermi model, the electron density distribution of a particular element and charge state is given by

$$n(x,q,Z_{\mathrm{n}}) = \frac{32}{9\pi^3}\cdot Z_{\mathrm{n}}^2\cdot\left[\frac{\varphi(x,q)}{x}\right]^{3/2}, \tag{9.1}$$

where

$$x = \frac{r}{r_{\mathrm{TF}}}, \tag{9.2}$$

$$r_{\mathrm{TF}} = \left(\frac{9\pi^3}{128}\right)^{1/3}\cdot\frac{1}{Z_{\mathrm{n}}^{1/3}} = 0.8853\cdot Z_{\mathrm{n}}^{-1/3}, \tag{9.3}$$

$$q = \frac{Z}{Z_{\mathrm{n}}}. \tag{9.4}$$

Z_{n} is the nuclear charge, Z the ion charge, q characterizes the ionization degree and r_{TF} is the Thomas–Fermi radius. The Thomas–Fermi function $\varphi(x,q)$ can be approximated by the Sommerfeld method (Sommerfeld 1932; Gombas 1949) which is an exact particular solution of the Thomas–Fermi differential equation:

$$\varphi(x,q) = \varphi(x)\cdot\left[1-\left(\frac{1+z(x)}{1+z_0(x)}\right)^{\lambda_1/\lambda_2}\right], \tag{9.5}$$

$$z(x) = \left(\frac{x}{144^{3/2}}\right)^{\lambda_2}, \tag{9.6}$$

$$z_0(x) = \left(\frac{x_0(q)}{144^{3/2}}\right)^{\lambda_2}, \tag{9.7}$$

$$\varphi_0(x) = \frac{1}{(1+z(x))^{\lambda_1/2}}, \tag{9.8}$$

$$\lambda_1 = 0.5\cdot\left(7+\sqrt{73}\right) = 7.77200, \tag{9.9}$$

$$\lambda_2 = 0.5\cdot\left(-7+\sqrt{73}\right) = 0.77200. \tag{9.10}$$

The reduced radius $x_0(q)$ is determined from the boundary condition

$$x_0\frac{\mathrm{d}\varphi(x_0)}{\mathrm{d}x} = -q. \tag{9.11}$$

In high-temperature plasma, i.e., when the ionization degree $q = Z/Z_{\mathrm{n}}$ is not too low, the reduced radius can be approximated by

$$x_0(q) = \begin{cases} 2.96 \cdot \left(\dfrac{1-q}{q}\right)^{2/3} & \text{if} \quad 0.2 < q \leq 1 \\ 6.84 \cdot \dfrac{1}{q^3} & \text{if} \quad q < 0.05 \end{cases}. \tag{9.12}$$

The ionization energy of an atom or ion is then given by

$$I_Z = Z_n^2 Ry \cdot \left\{ \left(\frac{128}{9\pi^2}\right)^{1/3} \cdot \frac{2 \cdot Z}{Z_n^{5/3} \cdot x_0(q, Z_n)} \right\}. \tag{9.13}$$

As can be seen from (9.13), the hydrogenic approximation $Z_n^2 \cdot Ry$ of the ionization potential of an ion with charge Z_n is corrected via the Thomas–Fermi electron density distribution that depends on nuclear charge and ionic charge [factor in parenthesis in (9.13)]. The comparison of the ionization energies obtained from (9.13) with detailed Hartree–Fock calculations shows a reasonable agreement for heavy elements over a wide range of ionization degrees (Demura 2015a, b). We note that certainly more accurate descriptions of the ionization potentials can be obtained from a direct fit to the vast amount of ionization potentials in dependence of Z and Z_n (Kirillow et al. 1975):

$$I_Z \approx 0.221 \cdot Ry \cdot \frac{(1+Z)^{4/3}}{1 - 0.96 \cdot \left(\dfrac{1+Z}{Z_n}\right)^{0.257}}. \tag{9.14}$$

Many modifications of the Thomas–Fermi model have been proposed in order to include shell structure, improve ionization energies, and in particular to approach the Hartree–Fock results for the electron density distribution (Dmitrieva and Plindov 1984; Fromy et al. 1996; Dyachkov et al. 2016). Also, modifications to derive the average degree of ionization in a dense plasma have been proposed (Ying and Kalman 1989). In addition, in order to improve the studies of the interaction of multielectron atoms with an electromagnetic field the classical kinetic Vlasov equations with self-consistent field has been proposed (Vinogradov and Tolstikhin 1989). It leads to improvement for the calculation of elementary processes, e.g., photoionization cross sections, and permits the calculation of the real part of the polarizability.

In the further developments to improve the statistical approach, one must not lose sight of the requirement that the fundamental equations of the statistical model of atoms, including the various corrections terms, should not be too complicated and, in any case, not more complicated than the basic equations of the quantum mechanical many-body approximation, e.g., the multiconfiguration Hartree–Fock methods. One must always bear in mind that the statistical theory of atoms is only a rough approximation of the quantum atom, and its advantage is its extreme simplicity both in structure and application to determine the electron and potential distributions of atoms, derive elementary processes in collisional–radiative regimes,

to shed light into the detailed atomic structure calculations (in particular for heavy atoms) and to derive general scaling laws that could be hardly obtained otherwise. It is this practical philosophy that we bear in mind when we consider (9.1)–(9.13) for the statistical framework of the atom/ion and the framework of the local plasma frequency (to be discussed further below) in order to enlarge the standard statistical Thomas–Fermi model also to elementary collisional–radiative processes and to the radiative properties of heavy atoms and ions in plasmas.

9.2 The Local Plasma Frequency Approximation

9.2.1 Oscillator Strengths Distribution and Photoabsorption

The response of an atom to an external field of given frequency ω can be conveniently discussed in terms of the properties of its differential oscillator strength distribution $f(\omega)$ that is directly related to the photoabsorption cross section of the atom:

$$\sigma(\omega) = \frac{2\pi^2 e^2}{m_e c} \cdot f(\omega). \tag{9.15}$$

The function $f(\omega)$ may be considered to comprise all the fundamental information on the quantum dynamics of atoms, but its quantum mechanical calculation is rather challenging and laborious. The distribution of the local atomic density determines a variety of elementary excitations with the classical plasma frequency. Concerning the Z_n- and frequency-dependence, we can identify three regions of interest. In the low-frequency range, where

$$0 \leq \frac{\hbar\omega}{Ry} \leq 1, \tag{9.16}$$

the function $f(\omega)$ essentially consists of the sharp lines familiar from optical spectroscopy separated by frequency ranges of low absorption while it changes irregularly with Z_n and reflects in its details the atomic binding. In the high-frequency range, where

$$\hbar\omega \geq Z_n^2 Ry, \tag{9.17}$$

the function $f(\omega)$ exhibits characteristic X-ray absorption edges. In the intermediate frequency range, where

$$1 \leq \frac{\hbar\omega}{Ry} \leq Z_n^2, \tag{9.18}$$

the contribution from intermediate shells of the atom is expected to overlap strongly and $f(\omega)$ becomes a smooth function on frequency. In this regime, excitations from intermediate atomic shells can be coupled rather strongly: new collective resonances of the atom as a whole become possible and a statistical approximation should apply best to the dynamics of the atom.

In the framework of the statistical approximation, the spectral distribution function $f(\omega)$ is derived from the general dynamic equations describing the density fluctuations induced in the atom by an external field. Using a local form of this framework, it is found that coherences between the motion in different parts of the atom causes modifications in $f(\omega)$ that can be formulated in terms of a dispersion denominator that identifies enhanced absorption as collective resonances of the atom as a whole (Brandt and Lundqvist 1965). The oscillation frequency is determined by the well-known formula for the electron plasma frequency

$$\omega(r) = \omega_{\mathrm{p}}(r) = \sqrt{\frac{4\pi e^2 n_{\mathrm{e}}(r)}{m_{\mathrm{e}}}}, \tag{9.19}$$

where $n_{\mathrm{e}}(r)$ is the local atomic electron density. $\omega_{\mathrm{p}}(r)$ is called the local plasma frequency LPF (see also Sect. 2.6). Comparison with the more general Vlasov approach shows that the LPF model does not take into account the polarization field induced by the external perturbation of the atomic electron density distribution (Vinogradov and Tolstikhin 1989). However, it turns out that the discrepancy between the LPF-statistical model for the photoionization cross sections is within the accuracy of calculations of radiative and collisional processes for multielectron ions by standard quantum mechanical codes and population kinetics (to be discussed below).

9.2.2 *Fermi Equivalent Photon Method and Local Plasma Oscillator Strength*

The interaction of the plasma electrons with a heavy atom can be considered within the framework of the Fermi approximation of equivalent photons (see Sect. 5.1). The electric field of the equivalent photon flux is determined by the Fourier expansion of the electric field of an electron, moving along with the classical trajectory in the field of the ion being excited. In this formulation, for example, the excitation of bound electrons in a multielectron ion is expressed in terms of the photoabsorption cross section of (9.15).

In quantum mechanics of atoms, almost all plasma physics relevant atomic characteristics can be approximated or expressed via the dipole oscillator strengths (see also Chaps. 2 and 7). It is therefore of particular interest for the generalization

of the applications of the plasma atom to derive an "effective plasma oscillator strengths." The determination of the classical oscillator strength follows from the correspondence principle (see also Chap. 2). In fact, if we consider the atom as a classical oscillator with an eigenfrequency equal to the local plasma frequency, we can readily derive its response on periodic (harmonic) perturbations. This determines the dynamic response of the classical oscillator and via correspondence with the quantum radiation emission we can identify a "plasma oscillator strength."

The simplest relation between the induced dipole moment and the local electrical field is given by

$$\vec{p}_{\text{induced}} = \alpha \cdot \vec{E}_{\text{local}} \tag{9.20}$$

(Note that the polarizability according to (9.20) is related to the quadratic Stark constant, see Sects. 7.4.2, 7.8.2). In the classical description, the frequency dependence of the oscillating atom under the action of a local electric field is given by

$$m_{\text{e}} \cdot \ddot{\vec{x}} + m_{\text{e}} \cdot \gamma \cdot \dot{\vec{x}} + m_{\text{e}} \cdot \omega_0^2 \cdot \vec{x} = q \cdot \vec{E}_{\text{local}} \cdot \exp(-i\omega t), \tag{9.21}$$

where $\vec{x}$ is the amplitude, m the mass, γ the damping constant, ω_0 the eigenfrequency of the oscillator, i.e., transition frequency, q the electric charge, and ω is the frequency of the local oscillating electric field. The stationary solution of (9.21) is given by

$$\vec{x}(t) = \frac{1}{\omega_0^2 - \omega^2 - i\gamma\omega} \cdot \frac{q}{m_{\text{e}}} \cdot \vec{E}_{\text{local}} \cdot \exp(-i\omega t). \tag{9.22}$$

Because the induced dipole moment is given by

$$\vec{p}_{\text{induced}} = q \cdot \vec{x}(t), \tag{9.23}$$

we obtain with the help of (9.20), (9.22), (9.23) for the dynamic polarizability

$$\alpha(\omega) = \frac{q^2}{m_{\text{e}}} \cdot \frac{1}{\omega_0^2 - \omega^2 - i\gamma\omega}. \tag{9.24}$$

Generalizing (9.24) to several oscillation frequencies, we obtain

$$\alpha(\omega) = \frac{q^2}{m_{\text{e}}} \cdot \sum_n \frac{1}{\omega_{0\text{n}}^2 - \omega^2 - i\gamma_{0\text{n}}\omega}. \tag{9.25}$$

If we separate the dynamic polarizability (9.24) in the real and imaginary part, i.e.,

$$\alpha(\omega) = \Re e(\alpha) + i\Im m(\alpha), \tag{9.26}$$

we obtain

$$\Re e(\alpha) = \frac{q^2}{m_e} \cdot \sum_n \frac{\omega_{0n}^2 - \omega^2}{\left(\omega_{0n}^2 - \omega^2\right)^2 + \gamma_{0n}^2 \omega^2}, \tag{9.27}$$

$$\Im m(\alpha) = \frac{q^2}{m_e} \cdot \sum_n \frac{\gamma \cdot \omega}{\left(\omega_{0n}^2 - \omega^2\right)^2 + \gamma_{0n}^2 \omega^2}. \tag{9.28}$$

For $\omega = 0$, the real part of the polarizability (9.25) corresponds to the static polarizability because the imaginary part (9.28) vanishes. In the local plasma frequency model, (9.25) has to be transformed to the continuous case (see also Sects. 2.3–2.6). In the spherical shell of thickness $\mathrm{d}r$, we encounter a confined charge of quantity $\mathrm{d}q = e \cdot 4\pi n_e(r)\, r^2 \mathrm{d}r$ and we obtain instead of (9.25):

$$\alpha(\omega) = \frac{4\pi e^2}{m_e} \cdot \int_0^{R_{atom}} \frac{n_e(r) r^2 \mathrm{d}r}{\omega_{0n}^2 - \omega^2 - i\gamma_{0n}\omega}, \tag{9.29}$$

where R_{atom} is the size of the atom. From (9.29), it follows with (9.19)

$$\alpha(\omega) = \int_0^{R_{atom}} \frac{\omega_p^2 \cdot r^2 \cdot \mathrm{d}r}{\omega_{0n}^2 - \omega^2 - i\gamma_{0n}\omega}. \tag{9.30}$$

Equation (9.29) can be readily compared with the quantum mechanical result for the polarizability, i.e.,

$$\alpha(\omega) = \frac{e^2}{m_e} \cdot \sum_n \frac{f_{0n}}{\omega_{0n}^2 - \omega^2 - i\gamma_{0n}\omega} \tag{9.31}$$

from which it follows that the term $4\pi n_e(r) r^2\, \mathrm{d}r$ can be interpreted as a local strengths in the LPF model, i.e., the local plasma oscillator strength

$$f_p(r) = 4\pi n_e(r) r^2\, \mathrm{d}r = f_{ij}. \tag{9.32}$$

The plasma oscillator strengths $f_p(r)$ are a central plasma atomic property that allows to deal with collisional–radiative elementary processes that are usually expressed in terms of the oscillator strengths f_{ij} for the transition $i \to j$. The Regemorter formula of electron collisional excitation according to (5.90)–(5.94) is

a typical example. In the LPF model, the indexes i, j are represented by the radial coordinate r and the radial interval dr [see right part of (9.32)]. From (9.32), it follows immediately that the plasma oscillator strengths fulfills the sum rule, i.e.,

$$\int \mathrm{d}f_{\mathrm{ij}} = Z_{\mathrm{n}} - Z = N_{\mathrm{e}}^{(\mathrm{bound})}. \tag{9.33}$$

9.3 Radiative Losses

9.3.1 General Relations

At low-density conditions, collisional excitation from the ground state to excited states decays readily by spontaneous radiative transitions (Corona model, see also Chap. 6) and the radiation losses are therefore determined by the collisional excitation rates itself. In the framework of the Fermi equivalent photon method, the radiation loss can therefore be expressed in terms of the photoexcitation rates in the field of equivalent photons (Demura et al. 2013, 2015a):

$$\begin{aligned} Q &= n_{\mathrm{e}}^{(\mathrm{free})} \int_0^{I/2Z_{\mathrm{n}}Ry} \mathrm{d}sRy \cdot \sigma_{\mathrm{ph}}(s) \cdot \left\langle \frac{\mathrm{d}I^{(\mathrm{Coulomb})}(s)}{\mathrm{d}s} \right\rangle_{\mathrm{E}} \\ &= n_{\mathrm{e}}^{(\mathrm{free})} \frac{4a_0 c\, Ry^2}{\sqrt{3\pi} \cdot e^2} \cdot \sqrt{\frac{Z_{\mathrm{n}}^2 Ry}{kT_{\mathrm{e}}}} \cdot \int_0^{I/2Z_{\mathrm{n}}Ry} \mathrm{d}s \cdot \sigma_{\mathrm{ph}}(s) \cdot \int_{\frac{2RyZ_{\mathrm{n}}}{kT_{\mathrm{e}}} \cdot s}^{\infty} \mathrm{d}u \cdot e^{-u} \cdot g(s,u) \end{aligned} \tag{9.34}$$

with

$$s = \frac{\hbar\omega}{2Z_{\mathrm{n}} \cdot Ry}, \tag{9.35}$$

$$u = \frac{E}{kT_{\mathrm{e}}}, \tag{9.36}$$

where a_0 is the Bohr radius, c the speed of light, e the electron charge, Ry the Rydberg energy, kT_{e} the thermal electron energy, $n_{\mathrm{e}}^{(\mathrm{free})}$ is the free electron density (note, that the atomic electron density is designated with $n_{\mathrm{e}}(r)$), I is the ionization potential of the ion with charge Z, and nuclear charge Z_{n}, σ_{ph} is the photoexcitation–photoionization cross section, $\left\langle \mathrm{d}I^{(\mathrm{Coulomb})}(s)/\mathrm{d}s \right\rangle_{\mathrm{E}}$ is the intensity of equivalent photon flux per unit of reduced frequency interval ds averaged over the energy E of the electron projectile scattered by the target and $g(s,u)$ is the Gaunt factor, describing the curvature of electron trajectory under its motion in the self-consistent

field of the heavy ion or atom. In the Coulomb approximation, the Gaunt factor becomes a function of the unique variable (Kogan et al. 1992):

$$v = Z_{\mathrm{eff}} \cdot Z_{\mathrm{n}} \cdot \left(\frac{Ry}{kT_{\mathrm{e}}}\right)^{3/2} \cdot \frac{s}{u^{3/2}}, \tag{9.37}$$

$$g(v) = \frac{\pi\sqrt{3}}{4} \cdot \left\{ iv H_{iv}^{(1)'}(iv) \cdot H_{iv}^{(1)}(iv) \right\} \approx \frac{\sqrt{6}}{\pi} \cdot \ln\left[\left(\frac{2}{\gamma v}\right)^{1/\sqrt{2}} + \exp\left(\pi/\sqrt{6}\right) \right], \tag{9.38}$$

where $H_{iv}^{(1)}(iv)$ and $H_{iv}^{(1)'}(iv)$ are Hankel functions and its first derivative with the argument iv, γ is the Euler constant ($\gamma = \exp(C) \approx 1.78$).

In the local plasma frequency model, the effective charge Z_{eff} from (9.37) is determined from the condition of equality of the Thomas–Fermi potential and the local Coulomb potential at the point $r_{\mathrm{s}} = x_{\mathrm{s}} \cdot r_{\mathrm{TF}}$ (r_{TF} is the Thomas–Fermi radius from (9.3)) that corresponds to the resonance condition of (9.19) expressed in terms of the reduced frequency s of (9.35):

$$Z_{\mathrm{eff}} = Z_{\mathrm{n}} \cdot \left\{ \varphi(x_{\mathrm{s}}, q) + \frac{q x_{\mathrm{s}}}{x_0} \right\}, \tag{9.39}$$

where $\varphi(x_{\mathrm{s}}, q)$, q and x are defined in (9.1)–(9.11). For low frequencies, the effective charge is equal to the ion charge Z, while in the high-frequency limit the effective charge is the nuclear charge Z_{n}. These limits are typically approximately approached for $s < 0.1$ (low-frequency limit) and $s > 30$ (high-frequency limit).

Taking into account only bound states, the first integration over frequencies in (9.34) extends up to the ionization threshold of the ion with charge Z while the second integration over energies of the incident electron corresponds to the excitation thresholds of atomic transitions in the statistical model. In the LPF approximation, the photoabsorption cross section is given by (see also (3.136) and (Rosmej et al. 2020a))

$$\sigma_{\mathrm{ph}}(\omega) = \frac{2\pi^2 e^2}{m_{\mathrm{e}} c} \cdot 4\pi r_\omega^2 \cdot \frac{n_{\mathrm{e}}(r_\omega)}{\left| \frac{\mathrm{d}\omega_{\mathrm{p}}(r)}{\mathrm{d}r} \right|} \tag{9.40}$$

or, expressed in terms of the Thomas–Fermi electron density:

$$\sigma_{\mathrm{ph}}(\omega) = \pi a_0^2 \cdot \frac{3\pi^3 e^2}{16\hbar c} \cdot \frac{s \cdot x_{\mathrm{s}}^2 \cdot \varphi(x_{\mathrm{s}}, q)}{|\varphi'(x_{\mathrm{s}}, q) - \varphi(x_{\mathrm{s}}, q)/x_{\mathrm{s}}|}. \tag{9.41}$$

Inserting (9.41) into (9.34), we obtain the final expression for the radiation loss in the Corona limit:

$$Q = n_{\mathrm{e}}^{(\mathrm{free})} \cdot \frac{\pi^3\sqrt{3\pi}\cdot a_0^3 Ry^2}{4} \cdot \sqrt{\frac{Z_{\mathrm{n}}^2 Ry}{kT_{\mathrm{e}}}} \cdot \int_0^{I/2Z_{\mathrm{n}}Ry} \frac{s\cdot x_{\mathrm{s}}^2\cdot\varphi(x_{\mathrm{s}},q)\cdot \mathrm{d}s}{|\varphi'(x_{\mathrm{s}},q)-\varphi(x_{\mathrm{s}},q)/x_{\mathrm{s}}|} \cdot \int_{\frac{2R_y Z_{\mathrm{n}}}{kT_{\mathrm{e}}}\cdot s}^{\infty} \mathrm{d}u\cdot e^{-u}\cdot g(s,u). \tag{9.42}$$

The radiation losses determined by (9.42) have been compared with detailed collisional–radiative modeling of tungsten over a wide range of temperatures (Demura 2015a), and it is found that (9.42) reproduces the rise of the radiation loss at small temperatures as well as the minima and maxima in the emission (that corresponds to the shell structure) at intermediate temperatures and the decrease at very high temperature. As concerns the absolute values of radiation loss, it is found that reasonable agreement is obtained setting $g(s,u)\approx 2$. At low temperatures, however, the agreement is limited because the Corona model is not quite valid due to the proximity of levels in low charged ions. Finally, we note that in order to compare (9.42) with the detailed collisional–radiative modeling it is necessary, to sum up the emission from (9.42) for every charge state and multiply with the respective relative population (normalized to one) of this charge state.

9.3.2 Density Effects

The Corona approximation of the radiation loss (9.42) described above is valid in the low-density high-temperature limit. As density increases and temperature decreases, the Corona approximation becomes invalid and has to be replaced by the general collisional–radiative model described in Chap. 6. In order to establish more general expressions for the radiation loss in the framework of the local plasma frequency approximation, let us first consider the Boltzmann limit (i.e., high-density limit). In the Boltzmann limit, direct and inverse processes are related to the principle of detailed balance that contains in the local plasma frequency approximation an equivalent Boltzmann exponential factor with the plasma frequency, i.e., $\exp(\hbar\omega_{\mathrm{P}}/kT_{\mathrm{e}})$.

Let us begin with the radiative terms expressed via the Einstein coefficients and the Fermi equivalent photon method. The Einstein coefficients describing the emission probability in terms of the emission oscillator strengths f_{if} of particular transitions $i\rightarrow j$ are given by

$$A_{\mathrm{ij}} = -2\frac{e^2}{mc^3}\,\omega^2 f_{\mathrm{ij}}. \tag{9.43}$$

The oscillator strengths in emission $f_{\mathrm{if}}<0$ and absorption $f_{\mathrm{ji}}>0$ are connected by the well-known relation

$$-g_{\mathrm{i}} f_{\mathrm{ij}} = g_{\mathrm{j}} f_{\mathrm{ji}}. \tag{9.44}$$

We also need to evaluate the contribution of induced emission or absorption, using correspondingly the following relations for the Einstein coefficients of induced emission

$$B_{\mathrm{ij}} = \frac{\pi^2 c^3}{\hbar\omega^3}\ A_{\mathrm{ij}} \tag{9.45}$$

and induced absorption

$$B_{\mathrm{ji}} = \frac{g_{\mathrm{i}}}{g_{\mathrm{j}}} \cdot \frac{\pi^2 c^3}{\hbar\omega^3}\ A_{\mathrm{ij}}. \tag{9.46}$$

Let $N_{\mathrm{EQP}}(\omega)$ the EQP number for a given frequency ω per unit frequency interval, $B_{\mathrm{ij}} \cdot N_{\mathrm{EQP}}(\omega)$ and $B_{\mathrm{ji}} \cdot N_{\mathrm{EQP}}(\omega)$ are the stimulated de-excitation and excitation rates corresponding to the EQP flux. Then from the equality for the direct and reverse processes, we obtain

$$B_{\mathrm{ij}}\, N_{\mathrm{EQP}}(\omega)\, N_{\mathrm{i}} = B_{\mathrm{ji}}\, N_{\mathrm{EQP}}(\omega)\, N_{\mathrm{j}}, \tag{9.47}$$

where N_{i}, N_{j} are the populations of levels i, j. For the Boltzmann distribution of level populations, i.e.,

$$N_{\mathrm{i}} = N_{\mathrm{j}} \exp[-\hbar\omega_{\mathrm{ij}}/kT_{\mathrm{e}}] \tag{9.48}$$

we obtain the following relation between direct and reverse processes

$$B_{\mathrm{ij}}\, N_{\mathrm{EQP}}(\omega)\ \exp[-\hbar\omega_{\mathrm{ij}}/kT_{\mathrm{e}}] = B_{\mathrm{ji}}\, N_{\mathrm{EQP}}(\omega). \tag{9.49}$$

On the other hand, the excitation rate under the influence of the EQP flux could be represented as the photoexcitation rate in terms of the photoabsorption cross section. The probability of induced radiation is determined by the product of the Einstein coefficient for induced radiation $B_{\mathrm{ij}}(\omega)$ and the radiation energy density $U_\sigma(\omega)$ (erg/cm^3) with the polarization σ. It is connected with the integral over solid angles Ω of the radiation spectral intensity $I_\sigma(\omega, k)$ with polarization σ in the direction, determined by the wave vector $\vec{k}$ and divided by the speed of light c:

$$\begin{aligned} \int \mathrm{d}\omega \cdot U_\sigma(\omega) \cdot B_{\mathrm{ij}}(\omega) &= \int \mathrm{d}\omega \cdot U_\sigma(\omega) \cdot \frac{\pi^2 c^3}{\hbar\omega^3} \cdot A_{\mathrm{ij}}(\omega) \\ &= \int \mathrm{d}\omega \left(\frac{1}{c} \int \mathrm{d}\Omega\, I_\sigma(\omega, \vec{k}) \right) \cdot \frac{\pi^2 c^3}{\hbar\omega^3} \cdot A_{\mathrm{ij}}(\omega). \end{aligned} \tag{9.50}$$

Assuming that the electrons have an unpolarized isotropic Maxwellian velocity distribution, the intensity of the EQP flux in the frequency interval $\mathrm{d}s = \mathrm{d}\omega \cdot (\hbar/2Z_{\mathrm{n}} \cdot Ry)$ (see (9.35)) produced in the elastic scattering of the electron

flux $n_e^{(free)} \cdot v_e$ (v_e is the electron thermal velocity of the free electrons) by the Coulomb center and averaged over the electron energy distribution could be expressed as

$$\left[\int d\Omega\, I_\sigma(\omega,\vec{k})\right]\cdot d\omega = \left[\int d\Omega\, I(\omega)\right]\cdot d\omega$$
$$= \left[n_e^{(free)} \cdot \frac{4a_0 cRy^2}{\sqrt{3\pi}\cdot e^2} \left(\frac{Z_n^2 Ry}{kT_e}\right)^{1/2} \int\limits_{\frac{2RyZ_n}{kT_e}\cdot s}^{\infty} du\, \exp[-u]\, g(s,u) \right]\cdot ds. \tag{9.51}$$

The photoabsorption cross section in the plasma model is given by (see also (3.135))

$$\sigma_{abs}(\omega) = \frac{2\pi^2 e^2}{m_e c}\int n_e(r)\cdot\delta\big(\omega-\omega_p(r)\big)\cdot d^3 r. \tag{9.52}$$

The integral in (9.52) is the sum over the oscillator strengths of all transitions, while a separate transition could be represented through the differential $d^3 r$ [see also comments related to (9.31)]:

$$d\sigma_{abs}(\omega) = \frac{2\pi^2 e^2}{m_e c}\, n_e(r)\,\delta\big(\omega-\omega_p(r)\big)\, d^3 r. \tag{9.53}$$

Let us now derive the probability of EQP induced absorption within the LPF model with the help of (9.43)–(9.53). We first transform the Einstein coefficient for induced radiation to the LPF model with the help of (9.19), (9.33), (9.43)–(9.51):

$$B_{ij} = \frac{\pi^2 c^3}{\hbar\omega^3}A_{ij} = \frac{2\pi^2 e^2}{m_e\omega} n_e(r)\, d^3 r\cdot\delta[\omega-\omega_p(r)]\cdot d\omega. \tag{9.54}$$

From (9.54), we obtain the Einstein coefficient of spontaneous emission:

$$A_{ij}(\omega) = 2\,\frac{e^2}{m_e c^3}\,\omega^2\, n_e(r)\,\delta[\omega-\omega_p(r)]\, d^3 r\cdot d\omega. \tag{9.55}$$

Therewith all Einstein coefficients could be represented in the statistical model in terms of the integral operators like in (9.52)–(9.55).

Then, in the two-state approximation for each pair of levels, we derive a population density balance equation for arbitrary free electron density $n_e^{(free)}$, equating the excitation rate via the EQP photoabsorption (from the lower state j) to the de-excitation rate via the spontaneous and EQP-induced radiative decay (from the upper state i):

$$N_j(r)\cdot\left[n_e^{(free)}\cdot\frac{2\pi^2a_0^3}{\sqrt{3\pi}}\left(\frac{Ry}{kT_e}\right)^{1/2}\frac{\omega_a}{\omega_p(r)}\int\limits_{u_{min}(r)}^{\infty}e^{-u}\,g\left(s_p(r),u\right)\cdot du\right]$$
$$=N_i(r)\cdot\left[n_e^{(free)}\cdot\frac{2\pi^2a_0^3}{\sqrt{3\pi}}\left(\frac{Ry}{kT_e}\right)^{1/2}\frac{\omega_a}{\omega_p(r)}\,e^{u_{min}(r)}\int\limits_{u_{min}(r)}^{\infty}e^{-u}\,g\left(s_p(r),u\right)\cdot du+\frac{2e^2}{m_ec^3}\cdot\frac{\omega_p^2(r)}{\omega_a}\right]$$

with

$$s_p(r)=\frac{\omega_p(r)}{Z_n\omega_a},\tag{9.57}$$

$$\omega_a=\frac{2Ry}{\hbar},\tag{9.58}$$

$$u_{min}(r)=\frac{\hbar\omega_p(r)}{kT_e}.\tag{9.59}$$

Note that $n_e^{(free)}$ is the total electron density of the free electrons that are scattered by the atom while $n_e(r)$ is the bound atomic electron density. Then the excited state population N_i depends on density and is expressed via the lower state one N_j as follows

$$N_i(r)=N_j(r)\cdot\frac{\int_{u_{min}(r)}^{\infty}e^{-u}g\left(s_p(r),u\right)du}{e^{u_{min}(r)}\int_{u_{min}(r)}^{\infty}e^{-u}g\left(s_p(r),u\right)du+\dfrac{\sqrt{3\pi kT_e}}{n_e^{(free)}\,\pi^2a_0^3\sqrt{Ry}}\cdot\dfrac{e^2}{m_ec^3}\cdot\dfrac{\omega_p^3(r)}{\omega_a^2}}.\tag{9.60}$$

From (9.60), we can see that it generalizes (9.48) for arbitrary densities. If the free electron density $n_e^{(free)}$ is very large, the second term in the denominator of (9.60) is very small compared with the first term and we obtain

$$N_i(r)=N_j(r)\cdot\exp(-u_{min}(r))=N_j(r)\cdot\exp\left(-\frac{\hbar\omega_p(r)}{kT_e}\right).\tag{9.61}$$

According to (9.19), the plasma frequency depends on the atomic density; therefore, according to (9.61) the Boltzmann relation $N_i(r)/N_j(r)$ of levels depends on radius. The radiation losses due to the transitions $i\rightarrow j$ (corresponding to the

local emission in the LPF model) can then be presented as an integral over frequencies using (9.55):

$$\int Q_{ij}(\omega, r) \cdot d\omega = \int \hbar\omega \cdot N_i(r) \cdot A_{ij}(\omega, r) \cdot d\omega = \frac{2\hbar e^2}{m_e c^3} \cdot N_i(r) \cdot \omega_p^3(r) \cdot n_e(r) \cdot d^3 r. \tag{9.62}$$

In order to obtain the radiation loss for one ion with nuclear charge Z_n and charge state Z, we express the excited state density in terms of the ground state density to relate the radiative emission to a certain number of ions in the spherical shell at radius r with thickness dr. Assuming that the excited state densities are negligible compared to the ground state densities, we can assume that $\sum_j N_j \approx N_Z$ where N_Z is the total density of ions with nuclear charge Z_n and charge state Z. Next, the total radiation loss $Q(Z_n, Z)$ is obtained from the sum of the contributions from all possible transitions. In the statistical model, the summation over contributions from the different transitions $i \to j$ consists in summing over the level populations N_j of different levels and integration over $d^3 r$. Therefore, the total radiation losses $Q(Z_n, Z)$ in the framework of an effective two-state approximation plasma model and Coulomb center effective charge take the form:

$$Q(Z_n, Z) = \frac{2\hbar e^2}{m_e c^3} \cdot \sum_i \int_0^{R_{atom}} N_i(r) \cdot \omega_p^3(r) \cdot n_e(r) \cdot d^3 r. \tag{9.63}$$

Substituting (9.60) into (9.62) and switching to the Thomas–Fermi dimensionless reduced radius x and expressing $n_e(x)$ and $\omega_p(x)$ via the Thomas–Fermi function $\varphi(x, q)$ (e.g., (9.5)), we obtain a generalized analytical formula for the total radiation loss per ion for arbitrary free electron density $n_e^{(free)}$ and electron temperature T_e:

$$\frac{Q(Z_n, Z)}{N_Z \cdot n_e^{(free)}} = \frac{4RyZ^3\omega_a}{n_e^{(free)}} \left(\frac{e^2}{\hbar c}\right)^3 \left(\frac{128}{9\pi^2}\right)^{3/2} \cdot \int_0^{x_0(q)} x^2 \cdot \left(\frac{\varphi(x, q)}{x}\right)^{15/4} \cdot G(x) \cdot R(x)\, dx \tag{9.64}$$

with

$$G(x) = \int_{u_{min}(x)}^{\infty} e^{-u} \cdot g(x, u) \cdot du, \tag{9.65}$$

$$R(x) = \frac{1}{\int_{u_{\min}(x)}^{\infty} e^{u_{\min}(x)-u} \cdot g(x,u) \cdot \mathrm{d}u + D\left(x, n_{\mathrm{e}}^{(\mathrm{free})}, T_{\mathrm{e}}, Z_{\mathrm{n}}, q\right)}, \tag{9.66}$$

$$D\left(x, n_{\mathrm{e}}^{(\mathrm{free})}, T_{\mathrm{e}}, Z_{\mathrm{n}}, q\right) = \frac{1}{n_{\mathrm{e}}^{(\mathrm{free})}} \cdot \left(\frac{128}{9\pi^2}\right)^{3/2} \cdot \left(\frac{e^2}{\hbar c}\right)^3 \cdot \frac{Z_{\mathrm{n}}^3}{\pi^2 a_0^3} \cdot \sqrt{\frac{3\pi k T_{\mathrm{e}}}{Ry}} \cdot \left(\frac{\varphi(x,q)}{x}\right)^{9/4}, \tag{9.67}$$

$$g(x,u) = g\left(\sqrt{\frac{Z_{\mathrm{eff}}^2 Ry}{kT_{\mathrm{e}}}} \cdot \frac{u_{\min}(x)}{2u^{3/2}}\right), \tag{9.68}$$

$$u_{\min}(x) = Z_{\mathrm{n}} \cdot \left(\frac{128}{9\pi^2}\right)^{1/2} \cdot \left(\frac{\varphi(x,q)}{x}\right)^{3/4} \cdot \left(\frac{2Ry}{kT_{\mathrm{e}}}\right). \tag{9.69}$$

Note that in (9.64)–(9.69), we have employed for consistency the Thomas–Fermi model for the ionization potential (9.13). In the limit of low free electron densities, (9.64)–(9.69) reproduce the result for the corona equilibrium; while in the opposite limit of high densities, the result corresponds to the Boltzmann distribution of atomic level populations.

The radiation losses of tungsten ions calculated from (9.64)–(9.69) are presented in Fig. 9.1 for different values of free electron density: 10^{14}, 10^{16}, 10^{18}, 10^{20} cm^{-3}. It is seen in Fig. 9.1 that these radiation losses are strongly suppressed with increase of plasma density in the region of low temperatures. This actually corresponds to the Boltzmann distribution of populations of excited states. When the second term

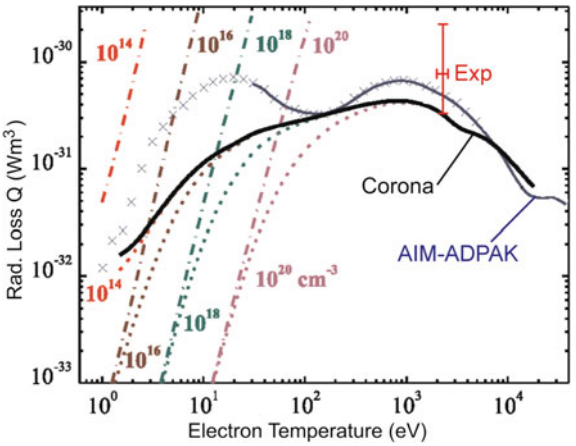

Fig. 9.1 Comparison of radiation losses from tungsten ions within the universal statistical approach with the numerical data from the AIM-ADPAK and ADPAK models

$D\left(x, n_e^{(free)}, T_e, Z_n, q\right)$ (9.67) in $R(x)$ from (9.66) (that corresponds to spontaneous emission), is much larger than the first one (corresponding to collisional de-excitation), we return to the results of the corona limit, shown in Fig. 9.1 by the solid black curve. In the opposite limit, when the de-excitation rate is much larger than the rate of spontaneous emission, (9.62)–(9.67) take the form:

$$\frac{Q(Z_n, Z)}{N_Z \cdot n_e^{(free)}} = \frac{4RyZ^3\omega_a}{n_e^{(free)}} \left(\frac{e^2}{\hbar c}\right)^3 \left(\frac{128}{9\pi^2}\right)^{3/2} \cdot \int_0^{x_0(q)} x^2 \cdot \left(\frac{\varphi(x,q}{x}\right)^{15/4} \cdot e^{-u_{min}(x)}\, dx. \tag{9.70}$$

This limit in the statistical approach is represented in Fig. 9.1 by "dashed-dot" curves for various densities 10^{14}, 10^{16}, 10^{18}, 10^{20} cm^{-3}. Such dependence corresponds to a near exponential increase of Q in the Boltzmann limit versus increasing electron temperature T_e. Asymptotically the "dotted" curves approach the Boltzmann limit at lower temperatures and the coronal limit at higher temperatures. This behavior is physically transparent. At low temperatures, the collisional de-excitation rate coefficients are rather high. Then, with density increase the de-excitation rates become larger than the spontaneous radiative decay, establishing the Boltzmann type of equilibrium. On the other hand, for large temperatures, the de-excitation rate coefficients decrease and then, with sufficiently low densities, the de-excitation rates become smaller than the spontaneous radiative decay rate. In this way, the coronal distribution of atomic populations is restored.

Let us now compare the results for the radiation loss calculated with the statistical approach with the detailed collisional–radiative model (see Chap. 6). Figure 9.1 depicts the results from collisional–radiative model calculations for tungsten (Kogan et al. 1992; Summers 1994; Post et al. 1977, 1995), blue crosses and solid blue curve indicated as "AIM-ADPAK". As already discussed in relation with the corona approximation of (9.42), the comparison of the total radiation losses with different models requests to sum up the line emission for every charge state. This implies a need for the calculation of the ionic charge state distribution (see also Chap. 6) to properly weight the radiation emission for each charge stage. In order to compare the statistical model of (9.64)–(9.69) with detailed collisional–radiative models, we employ the charge state distribution proposed by Post (1977). It can be seen that the corona limit of the universal statistical approach (9.64)–(9.69) provides a reasonable approximation of the radiation losses within a factor of two in the temperature interval from about 50–30.000 eV. For lower temperatures, the emission peak near about 20 eV is not well reproduced. In this temperature range, the atomic configurations are very complex and important deviations from the corona model are encountered as discussed in relation with (9.70). It should be noted that the precise determination of the ionic populations and the total loss rates for heavy elements in dependence of temperature and density is a very complex

problem that is controversy discussed up to present days in particular if M- and N-shells are involved (Beiersdorfer et al. 2012; Scott and Hansen 2010; Piron et al. 2017). For example, average charge states $\langle Z \rangle$ of gold at about 1 keV temperature at densities around 10^{21} cm^{-3} may differ as much as 10 for different calculations (Scott and Hansen 2010) while it should be remembered that a change in average charge state of only $\langle \Delta Z \rangle = 1$ results in an entirely different spectral distribution. Moreover, high precision experiments are likewise very difficult, as independent temperature, density, and charge state measurements are requested. For demonstration, Fig. 9.1 contains the experimental measurement of the radiation loss of tungsten (Pütterich et al. 2010). The experimental error bars are of the same order as the differences of different model calculations (Demura et al. 2015a; Pütterich et al. 2010).

Radiation loss related to radiative recombination and dielectronic recombination is much lower than the total radiation loss in the depicted temperature interval (Pütterich et al. 2010). Although the direct radiation loss related to dielectronic recombination is not very important for the total radiation loss, it is very important for the correct account of the ionization charge state distribution that in turn influences on the total radiation loss.

The statistical model for arbitrary density according to (9.64)–(9.69) represents therefore a useful approximation of the radiation loss for each charge state. Due to the Thomas–Fermi model approximation, (9.64)–(9.69) provide a generalized unified analytical description of the radiation loss for any heavy ion and allow to study in a transparent manner several physical properties of the line radiation loss. However, currently there exists no well-established theory to extend the statistical model to a generalized analytical description that includes also the ionic charge state distribution (resulting in a self-consistent total radiation loss calculation). Below, we discuss their essential ingredients, namely the statistical approach to ionization and dielectronic recombination.

Finally we note that for very high densities, the Thomas–Fermi atom size can become comparable of the ionic interparticle distance, such that the boundary condition at the periphery of the atomic electron density distribution could change. This would change the behavior of the distribution itself. This effect is strongly related to the ionization potential depression discussed in Chap. 8 and Annex A.4 and not specific to the statistical model but related to all types of collisional–radiative modeling.

9.4 Statistical Ionization Cross Sections and Rates

We now show that the statistical approach allows one to obtain the expressions for the total electron impact single ionization cross sections of multielectron ions and related ionization rates. Indeed, instead of the intensity of equivalent photons we can operate with the number of equivalent photons $\dfrac{\mathrm{d}N(\omega)}{\mathrm{d}(\omega/\omega_\mathrm{a})}$ at given frequency ω

in the unit frequency interval $d\omega$ in unit time interval at the fixed incident electron energy E, which in the dimensionless form could be determined by the expression (compare with (9.40), (9.41))

$$\frac{dN(\omega)}{d(\omega/\omega_a)} = \left(\frac{c\hbar}{e^2}\right) \cdot \frac{1}{2\sqrt{3}} \cdot \frac{\omega_a}{\omega} \cdot \left(\frac{Ry}{E}\right) \cdot g\left(Z, \left(\frac{Ry}{E}\right)^{3/2}, \frac{\omega}{\omega_a}, Z_n\right). \tag{9.71}$$

Multiplying the number of EQP (9.51) by the photoionization cross section and integrating over s from the reduced ionization potential $I_Z/(2RyZ_n)$ up to the reduced energy of electron projectile $E/(2RyZ_n)$, we arrive in the Coulomb approximation (9.37), (9.38) to the following expression for the electron ionization cross section

$$\sigma_i(E) = \frac{\pi^4 a_0^2 \sqrt{3}}{32} \cdot \frac{Ry}{E} \cdot \int_{I_i/(2RyZ_n)}^{E/(2RyZ_n)} g\left[Z_{eff} Z_n \left(\frac{Ry}{E}\right)^{3/2} \cdot s\right] \cdot \frac{x_s^2 \varphi(x_s, q) \cdot ds}{|\varphi'(x_s, q) - \varphi(x_s, q)/x_s|}. \tag{9.72}$$

The corresponding statistical ionization rates are obtained by averaging the ionization cross section of (9.72) over the Maxwellian energy distribution. This can conveniently be performed by changing the sequence of integration and firstly integrate over energies of the incident plasma electrons. This average concerns in fact only the total flux of EQP number $n_e^{eff} \upsilon_e \frac{dN(\omega)}{d\omega}$ ($n_e^{(free)}$ is the plasma electron density, and υ_e is the corresponding thermal electron velocity). Then, the ionization rate could be expressed as

$$R_i(Z_n, q, T_e) = n_e^{(free)} \frac{a_0^3 \omega_a \pi^3 \sqrt{3\pi}}{16} \sqrt{\frac{Ry}{kT_e}} \cdot \left\{ \int_{\frac{I_Z}{2Z_n Ry}}^{\infty} \frac{x_s^2 \varphi(x_s, q) \cdot ds}{|\varphi'(x_s, q) - \varphi(x_s, q)/x_s|} \right\} \cdot \left\{ \int_{\frac{2Z_n Ry}{kT_e} \cdot s}^{\infty} e^{-u} \cdot g(v) \cdot du \right\}, \tag{9.73}$$

where v is defined by (9.37).

Figure 9.2 shows the ionization cross section for an open 4*f*-shell of a heavy element, the tungsten W^{9+} ion, calculated with the statistical model of (9.72). Also presented in Fig. 9.2 are the experimental data from (Stenke et al. 1995) and relativistic excitation–autoionization distorted wave calculations (Loch et al. 2005).

Figure 9.2 demonstrates that the statistical model describes the experimental data within a factor of two from threshold to high energies. The threshold for heavy elements requests particular attention because excitation–autoionization as well as excitation from metastable levels is of importance. It is very cumbersome to include all necessary excitation–autoionization channels in a fully quantum approach, as branching factors (for radiative and autoionization decay) have to be involved. In this respect, the statistical model is very convenient because the statistical model includes both direct and indirect contributions to ionization. Moreover, it is likewise difficult in experiment, to measure pure direct excitation cross sections because the electron beam results likewise in the excitation of metastable levels (highly populated) from which ionization can also proceed.

Let us now consider ionization rates from open 4*d*-shell and open 4*p*-shell configurations of Xe^{12+} and Xe^{20+}, respectively, and compare the statistical ionization rate coefficients of (9.73) with quantum mechanical calculations in the Coulomb–Born exchange approximation of the direct ionization rate using Vainshtein's ATOM code (Vainshtein and Shevelko 1986; Sobelman and Vainshtein 2006; Povyshev et al. 2001).

As can be seen from Fig. 9.3, also quite good agreement between the statistical model and the quantum calculation are obtained. For low electron temperatures, i.e., when the effective ionization cross sections are near threshold, the quantum cross sections provide systematically lower rates than the statistical model because the depicted quantum calculations do include only the direct cross section.

Numerous comparisons with experimental data and different methods of rather complex quantum mechanical ionization cross sections have been performed (Demura et al. 2015b) and it is found that the statistical approach to ionization cross sections constitutes an efficient and rather precise method for heavy elements and permits easily inclusion of direct and indirect ionization contributions.

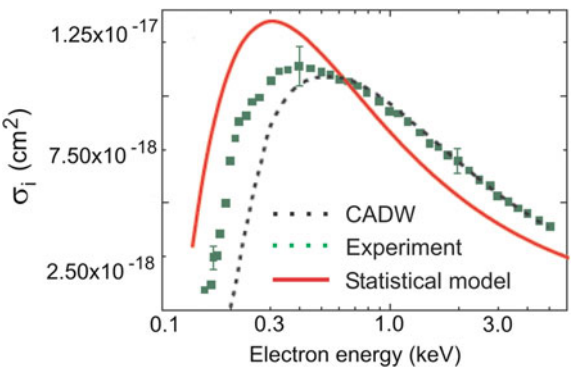

Fig. 9.2 Comparison of the ionization cross section of tungsten W^{9+} ions with experimental data (Stenke et al. 1995) and complex collisional excitation–autoionization distorted wave calculations (Loch et al. 2005)

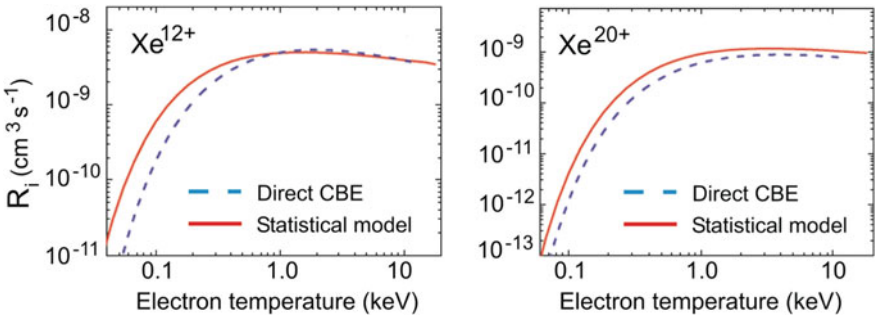

Fig. 9.3 Comparison of the ionization cross section of Xeon ions with the quantum mechanical calculations in Coulomb–Born exchange approximation for the direct ionization rate

9.5 Statistical Dielectronic Recombination Rates

Dielectronic recombination (see also Chap. 5 and review (Rosmej et al. 2020b)) is the most effective recombination channel in electron–heavy ion collisions. Due to the complex electronic structure of multielectron ions, the proper account of all necessary channels is a very difficult task, in particular for open shell configurations. In addition, in dense plasmas, dielectronic capture might effectively proceed from excited states (see also Chap. 5) that considerably increases the quantum channels for the dielectronic capture. Moreover, in heavy ions, numerous metastable states may play the role of excited states even in rather low-density plasmas, thereby increasing the numerical complexity of fully quantum calculations considerably. At present, the dielectronic recombination of heavy ions is still under controversial discussion and is one of the main sources of discrepancies between different methods of calculations for radiation loss and ionic charge state distributions. It is therefore of great interest to develop different methods for the calculation of the dielectronic recombination in heavy ions that permit more general studies including the analysis of scaling laws. As has been demonstrated in the foregoing paragraphs, the statistical approach provides reasonable approximations not only for the atomic structure, but for the calculations of elementary processes too. We are therefore seeking to extend the approach of the local plasma frequency approximation also to the dielectronic recombination.

9.5.1 General Formula

The general formula for the total dielectronic recombination rates DR can be written as Sobelman and Vainshtein (2006)

$$Q_{\mathrm{DR}}(T) = \left(\frac{4\pi Ry}{kT_{\mathrm{e}}}\right)^{3/2} a_0^3 \frac{g_{\mathrm{f}}}{g_{\mathrm{i}}} \cdot W_{\mathrm{R}} \cdot \sum_{n,l} \left\{ \frac{W_{\mathrm{A}}(n,l)}{W_{\mathrm{R}} + W_{\mathrm{A}}(n,l)} \cdot \exp\left(-\frac{\hbar\omega}{kT_{\mathrm{e}}} + \frac{Z_{\mathrm{i}}^2 Ry}{n^2 kT_{\mathrm{e}}} \right) \right\}, \tag{9.74}$$

where kT_{e} is the electronic temperature in [eV], $Ry = 13.61\,\mathrm{eV}$, g_{i} and g_{f} are the statistical weights of the initial and final states of the atomic core, respectively. W_{R} is the radiative transition probability inside the core, W_{A} is the autoionization decay rate of an excited atomic energy level, $\hbar\omega$ is the transition energy inside the core, Z_{i} is the ion charge, a_0 is the Bohr radius, and n, l are the principle and orbital quantum numbers of the captured electron, respectively. The radiative decay rate is expressed simply in terms of the oscillator strength f_{ij} for the transition inside the core (c is the speed of light):

$$W_{\mathrm{R}} = \frac{2\omega^2 f_{\mathrm{if}}}{c^3}. \tag{9.75}$$

In order to obtain the expression for the autoionization decay rate $W_{\mathrm{A}}(n,l)$, we use a relationship between the decay rate $W_{\mathrm{A}}(n,l)$ and the partial electron excitation cross section $\sigma_{\mathrm{ex}}(l)$ at threshold in the semiclassical representation. The quantities $W_{\mathrm{A}}(n,l)$ and $\sigma_{\mathrm{ex}}(l)$ describe the mutually inverse processes, so the relationship between them can be obtained from the detailed balance (see also Sect. 7.7.2) between ions $X^{Z_{\mathrm{i}}+1}$ and $X^{Z_{\mathrm{i}}}$. Thus, we obtain

$$(2l+1) g_{\mathrm{f}} W_{\mathrm{A}}(n,l) = \frac{Z_i^2}{n^3} \omega g_{\mathrm{i}} \frac{\sigma_{\mathrm{ex}}(l)}{\pi^2 a_0^2}. \tag{9.76}$$

The electron excitation cross section in the semiclassical approximation takes the form

$$\sigma_{\mathrm{exc}}(l) = \frac{8\pi}{3} \left(\frac{\hbar}{m_e \upsilon_{\mathrm{e}}}\right)^2 \frac{g_{\mathrm{f}}}{g_{\mathrm{i}}} f_{\mathrm{if}} Z_{\mathrm{i}}^{-2} (l+1/2)^2 G\left(\frac{\omega (l+1/2)^3}{3Z_{\mathrm{i}}^2} \right), \tag{9.77}$$

where the function $G(u)$ is given by ($K_{1/2}$ and $K_{3/2}$ are the Mcdonald functions)

$$G(u) = u \cdot \left(K_{1/3}^2(u) + K_{2/3}^2(u) \right). \tag{9.78}$$

Taking into account that the essential values of the argument of the $G(u)$ function are never close to zero, it is possible to replace $G(u)$ by its asymptotic expansion:

$$G(u) \approx 3.4 \cdot \exp(-2u). \tag{9.79}$$

Within these approximations, the autoionizing decay rate takes the form:

$$W_{\mathrm{A}}(n,l) = 0.72 \cdot \frac{\omega(l+0.5) f_{\mathrm{ij}}}{n^3} \cdot \exp\left(-\frac{2\omega(l+0.5)^3}{3Z_{\mathrm{i}}^2}\right). \tag{9.80}$$

The sum of the oscillator strengths satisfies the Thomas–Reiche–Kuhn sum rule, i.e.,

$$N_{\mathrm{e}}^{\mathrm{bound}} = \sum_f f_{\mathrm{if}}. \tag{9.81}$$

As discussed in the foregoing paragraphs, the oscillator strengths in the statistical model are expressed in terms of the atomic electron density $n_{\mathrm{e}}(r,q,Z_{\mathrm{n}})$ (9.32) and the statistical sum rule is given by ($N_{\mathrm{e}}^{\mathrm{bound}}$ is the total number of bound electrons)

$$N_{\mathrm{e}}^{\mathrm{bound}} = \int n_{\mathrm{e}}(r,q,Z_{\mathrm{n}})\mathrm{d}V. \tag{9.82}$$

The application of the semiclassical statistical model to the general formula (9.72) for the total DR is achieved by application of the relationships

$$\sum_f f_{\mathrm{if}} \rightarrow \int_0^{r_0} \mathrm{d}r \cdot 4\pi r^2 n_{\mathrm{e}}(r,q,Z_{\mathrm{n}}) \tag{9.83}$$

and

$$E_{\mathrm{if}} \rightarrow \omega = \sqrt{4\pi n_{\mathrm{e}}(r,q,Z_{\mathrm{n}})}. \tag{9.84}$$

After all substitutions, we obtain for the DR rates:

$$Q_{\mathrm{DR}}(\mathrm{cm}^3/\mathrm{s}) = 0.61 \times 10^{-8} \cdot Q_{\mathrm{DR}}(a.u), \tag{9.85}$$

$$Q_{\mathrm{DR}}(a.u.) = \frac{54.5}{T_{\mathrm{e}}^{3/2}}\left(\frac{Z_{\mathrm{n}}}{Z_{\mathrm{i}}}\right)^2 \cdot \int_0^{x_0} \mathrm{d}x\, x^2 \left(\frac{\varphi(x)}{x}\right)^{9/4} \times \int_1^{\infty} \mathrm{d}t\, \exp\left(-\frac{\omega(x)}{T_{\mathrm{e}}}\left(1-\frac{1}{t^2}\right)\right) \int_0^{l_{\max}=t\cdot n_1-1} \mathrm{d}l \frac{(l+0.5)\exp\left[-2\omega(x)(l+0.5)^3/3Z_{\mathrm{i}}^2\right]}{t^3 + A(x,l)}, \tag{9.86}$$

$$A(x,l) = 5.2 \times 10^6 (l+0.5) \frac{\exp\left[-2\omega(x)(l+0.5)^3/3Z_{\mathrm{i}}^2\right]}{Z_{\mathrm{i}}^3\sqrt{\omega(x)}}, \tag{9.87}$$

$$\omega(x) = 1.2 \cdot Z_{\mathrm{n}} \cdot \left(\frac{\varphi(x)}{x}\right)^{3/4} \tag{9.88}$$

with $T_{\mathrm{e}}(a.u.) = T_{\mathrm{e}}(\mathrm{eV})/27.21$ and $t = n/n_1$, where n_1 is a minimal possible quantum number. n_1 is the lowest level, on which electron capture is possible and corresponds to an energy of an incident electron E_{i}

$$E_{\mathrm{i}} = \omega - \frac{Z_{\mathrm{i}}^2}{2n^2} \tag{9.89}$$

that is equal to zero, i.e.,

$$0 = \omega - \frac{Z_{\mathrm{i}}^2}{2n_1^2}. \tag{9.90}$$

From (9.90), it follows

$$n_1 = \frac{Z_{\mathrm{i}}}{\sqrt{2\omega}}. \tag{9.91}$$

9.5.2 *Orbital Quantum Number Averaged Dielectronic Recombination Rates*

In the simplest version of the statistical model, the atomic density, excitation energies, and oscillator strengths do not depend on the orbital momentum quantum number l. If we average the branching factor over orbital momentum we obtain for the total dielectronic recombination rate:

$$Q_{\mathrm{DR}}(a.u.) = \frac{39.2}{T_{\mathrm{e}}^{3/2}}\left(\frac{Z_{\mathrm{n}}}{Z_{\mathrm{i}}}\right)^2 \frac{Z_{\mathrm{n}}}{Z_{\mathrm{i}}^2} \int_0^{x_0} \mathrm{d}x \cdot x^2 \left(\frac{\varphi(x)}{x}\right)^3 \int_1^{\infty} \frac{\mathrm{d}t}{t^2} \exp\left(-\frac{\omega(x)}{T}\left(1 - \frac{1}{t^2}\right)\right) \times \int_0^{l_{\max}=t\cdot n_1-1} \mathrm{d}l \frac{(l+0.5)^2 \exp\left[-2\omega(x)(l+0.5)^3/3Z_{\mathrm{i}}^2\right]}{t^3 + A(x,l)}, \tag{9.92}$$

where the function $A(x,l)$ is given by (9.87), (9.88). Instead of averaging over the branching factor, we may investigate averaging the autoionization decay rate [3] from (9.80) over orbital quantum number, i.e.,

$$\langle W_{\mathrm{A}}(n,l)\rangle = 1.7\frac{f_{\mathrm{if}}Z_{\mathrm{i}}^2}{\pi n^5\omega}. \tag{9.93}$$

For the corresponding total dielectronic recombination rate, we then obtain

$$\begin{aligned} Q_{\mathrm{DR}}(a.u.) = {} & \frac{0.86\times 10^2}{T_{\mathrm{e}}^{3/2}}\left(\frac{Z_{\mathrm{n}}}{Z_{\mathrm{i}}}\right)^2 \int_0^{x_0} \mathrm{d}x\cdot x^2\left(\frac{\varphi(x,q)}{x}\right)^{9/4} \\ & \times \int_1^{\infty} \mathrm{d}t \frac{\exp\left[-\dfrac{1.2Z}{T_{\mathrm{e}}}\left(\dfrac{\varphi(x,q)}{x}\right)^{3/4}\left(1-\dfrac{1}{t^2}\right)\right]}{t^5+A(x)}, \end{aligned} \tag{9.94}$$

$$A(x) = \frac{4.56\times 10^6}{Z_{\mathrm{i}}^3\sqrt{Z_{\mathrm{n}}}\left(\dfrac{\varphi(x,q)}{x}\right)^{3/8}}. \tag{9.95}$$

9.5.3 Statistical Burgess Formula

It is of great interest to apply the statistical approach to the Burgess-Mertz formula (Burgess 1964; Cowan 1981) for dielectronic recombination because this formula is widely employed and cast into an entirely analytical expression (z is the spectroscopic symbol $z = Z_n - N_e^{(\mathrm{bound})} + 1$, while $Z_i = Z_n - N_e^{(\mathrm{bound})}$ is the ion charge, see also eqs. (5.138)–(5.143)):

$$Q_{\mathrm{DR}}\ (\mathrm{cm}^3/\mathrm{s}) = 10^{-13}B_{\mathrm{d}}\cdot\beta^{3/2}\cdot e^{-\beta\cdot\chi_{\mathrm{d}}}, \tag{9.96}$$

$$B_{\mathrm{d}} = 480\, f_{\mathrm{if}}\left[\frac{z\chi}{z^2+13.4}\right]^{3/2}[1+0.105(z+1)\chi+0.015(z+1)^2\chi^2]^{-1}, \tag{9.97}$$

$$\beta = \frac{(z+1)^2 Ry}{kT_{\mathrm{e}}}, \tag{9.98}$$

$$\chi_{\mathrm{d}} = \frac{\chi}{1+0.015\dfrac{z^3}{(z+1)^2}}, \tag{9.99}$$

$$\chi = \frac{E_{\mathrm{if}}}{(z+1)^2 Ry}. \tag{9.100}$$

The statistical version of the Burgess-Mertz formula is obtained, going from the oscillator strength in (9.97) to the electron density and from the energy difference in (9.100) to the plasma frequency employing (9.83) and (9.84), respectively. After transformation to dimensionless variables, we obtain:

$$Q_{\mathrm{DR}}(\mathrm{cm}^3/\mathrm{s}) = 10^{-13}\beta^{3/2}\int_0^{x_0} \mathrm{d}x \cdot x^2 B_{\mathrm{d}}(x) e^{-\beta\chi_{\mathrm{d}}(x)}, \tag{9.101}$$

$$B_{\mathrm{d}}(x) = \frac{135\pi^3}{Z_n} n(x,q,Z_n)\left[\frac{z\chi(x)}{z^2+13.4}\right]^{1/2}\frac{1}{A(x)}, \tag{9.102}$$

$$A(x) = 1 + 0.105(z+1)\chi(x) + 0.015(z+1)^2\chi^2(x), \tag{9.103}$$

$$\chi(x) = \frac{2}{(z+1)^2}\sqrt{4\pi n_{\mathrm{e}}(x,q,Z)}, \tag{9.104}$$

$$\chi_{\mathrm{d}}(x) = \frac{\chi(x)}{1 + 0.015\dfrac{z^3}{(z+1)^2}}. \tag{9.105}$$

9.5.4 Statistical Vainshtein Formula

Several improvements to the Burgess formula have been proposed in the literature (see also Chap. 5). In this respect, it should be remembered that the Burgess formula is of interest due to its generality and great simplicity. The main drawback of the Burgess formula is the single channel approach that could result in considerable overestimation of the total dielectronic recombination rate (see Sect. 5.6.2.1). The multichannel approach requests usually complex atomic structure calculations that are very difficult to realize for heavy atoms. One of the most efficient general improvements of the Burgess formula including a simplified multichannel approach has been proposed by Vainshtein (Beigman et al. 1981; Sobelman and Vainshtein 2006) (see also Chap. 5). In the single channel approach, the Vainshtein formula can be summarized as follows:

$$Q_{\mathrm{DR}}\ (\mathrm{cm}^3/s) = 10^{-13} B_{\mathrm{d}} \beta^{3/2} e^{-\dfrac{\Delta E_{\mathrm{fi}}}{T}}, \tag{9.106}$$

$$B_{\mathrm{d}} = C' \frac{z}{n_1^4} f_{\mathrm{if}} \sum_{n > n_1} e^{\delta\beta} \sum_{l<n} \frac{2l+1}{1 + \left(\dfrac{n}{n_{\mathrm{s}}}\right)^3}, \tag{9.107}$$

$$n_{\rm s} = n_{\rm s}(l) = 137\left[\frac{n_1^2\sigma_{\rm if}(l)}{\pi^2 a_0^2(2l+1)f_{\rm if}}\right]^{1/3}, \tag{9.108}$$

$$\delta\beta = \frac{z^2 Ry}{n^2 kT_{\rm e}}, \tag{9.109}$$

$$C' = 10^{13}\frac{4\pi^{3/2}a_0\hbar}{(137)^3 m_e}\left(\frac{z}{z+1}\right)^3 = 0.53\left(\frac{z}{z+1}\right)^3, \tag{9.110}$$

where $\Delta E_{\rm fi}$ is the energy difference between initial i and final f levels, and $\sigma_{\rm if}(l)$ is the partial excitation cross section at threshold. Implementation of the multichannel approach results into a modification of the $B_{\rm d}$ factor, i.e.,

$$B_{\rm d}^{\rm (multi-channel)} = C'\frac{z}{n_1^4}f_{\rm if}\sum_{n>n_1}e^{\delta\beta}\sum_{l<n}\frac{2l+1}{B+\left(\frac{n}{n_{\rm s}}\right)^3} \tag{9.111}$$

with

$$B = \sum_{f'}\frac{\Delta E_{\rm ff'}}{\Delta E_{\rm fi}}\cdot\frac{g_{\rm f'}}{g_{\rm i}}\cdot\frac{\sigma_{\rm f'f}(l)}{\sigma_{\rm if}(l)} \tag{9.112}$$

that results into an effective reduction of the branching factor (Beigman et al. 1981). Undertaking the substitutions of (9.83), (9.84) and replacing the sum over nl by integrations, we obtain from (9.106)–(9.110):

$$Q_{\rm DR}(a.u.) = \frac{13.6}{T_{\rm e}^{3/2}}\left(\frac{Z_{\rm n}}{Z_{\rm i}}\right)^2\int_0^{x_0}{\rm d}x\cdot x^2\left(\frac{\varphi(x)}{x}\right)^{9/4}\int_1^{\infty}{\rm d}t\,\exp\left(-\frac{\omega(x)}{T_{\rm e}}\left(1-\frac{1}{t^2}\right)\right)$$
$$\times\int_0^{l_{\rm max}=t\cdot n_1-1}{\rm d}l\frac{(l+0.5)^2\exp\left(-\dfrac{2\omega(x)(l+0.5)^3}{3Z_{\rm i}^2}\right)}{t^3+A(x,l)}, \tag{9.113}$$

$$A(x,l) = 1.3\times10^6(l+0.5)\frac{\exp\left[-2\omega(x)(l+0.5)^3/3Z_{\rm i}^2\right]}{Z_{\rm i}^3\sqrt{\omega(x)}}, \tag{9.114}$$

$$\omega(x) = 1.2Z_n\left(\frac{\varphi(x)}{x}\right)^{3/4}. \tag{9.115}$$

If we average (9.102)–(9.114) over the orbital angular electron momentum l and replace the sum over l by an integration, we obtain:

$$Q_{\mathrm{DR}}(a.u.) = \frac{98.1}{T_{\mathrm{e}}^{3/2}}\left(\frac{Z_{\mathrm{n}}}{Z_{\mathrm{i}}}\right)^2 \frac{Z_{\mathrm{n}}}{Z_{\mathrm{i}}^2}\int_0^{x_0} \mathrm{d}x \cdot x^2 \left(\frac{\varphi(x)}{x}\right)^3 \int_1^{\infty} \frac{\mathrm{d}t}{t^2} \exp\left(-\frac{\omega(x)}{T}\left(1-\frac{1}{t^2}\right)\right) \times \int_0^{l_{\max}=t\cdot n_1-1} \mathrm{d}l \frac{(l+0.5)^3 \exp\left(-\dfrac{2\omega(x)(l+0.5)^3}{3Z_{\mathrm{i}}^2}\right)}{t^3 + A(x,l)}, \tag{9.116}$$

$$A(x,l) = 5.2 \times 10^6 (l+0.5) \frac{\exp\left[-2\omega(x)(l+0.5)^3/3Z_{\mathrm{i}}^2\right]}{Z_{\mathrm{i}}^3 \sqrt{\omega(x)}}, \tag{9.117}$$

$$\omega(x) = 1.2 Z_n \left(\frac{\varphi(x)}{x}\right)^{3/4}. \tag{9.118}$$

9.5.5 *Numerical Comparison of Different Dielectronic Recombination Models*

For heavy ions, the quantum mechanical level-by-level calculations are very complex and have so far mainly been carried out for closed shell configurations. Only recently, also open shell configurations have been considered (Balance et al. 2010; Wu et al. 2015). In open shell configuration (such as the open 4*p*-, 4*d*-, 4*f*-shells or even higher ones like the 5*p*-, 5*d*-, 5*f*-, 5*g*-shells), excitation–autoionization channels are very complex and the overall completeness of quantum mechanical level-by-level calculations should still be considered with care. The analysis shows that order of magnitude disagreements can be excepted for low temperatures while for high temperatures, different level-by-level quantum mechanical models differ by about a factor of 2 while the Burgess-Mertz approach may deviate by many orders of magnitude providing also an entirely inadequate temperature dependence (Behar et al. 1996).

Let us compare first the various statistical approaches with detailed quantum level-by-level calculations. Figure 9.4 shows statistical dielectronic recombination rates *nl*-resolved according to (9.85)–(9.88), curve designated as "Statistical *nl*"; the statistical DR rate with orbital average of the branching factor according to (9.92), curve designated as "Statistical *n*"; the statistical approach with orbital average of the autoionization rate according to (9.94), (9.95), curve designated as "Statistical *W(n)*"; the Burgess DR rate according to (9.96)–(9.100), (9.101)–(9.105), curve

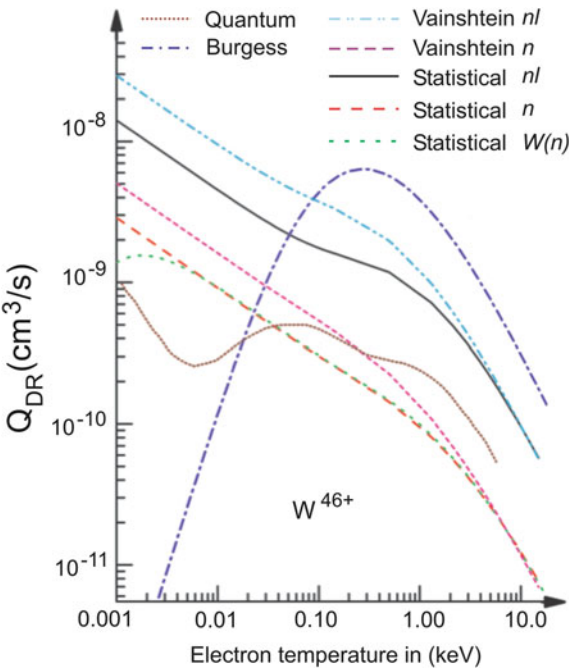

Fig. 9.4 Comparison of different statistical approaches with quantum level-by-level calculations for the Ni-like sequence $3s^2 3p^6 3d^{10}$ of tungsten W^{46+}

designated as "Burgess"; the Vainshtein approach according to (9.106)–(9.110), (9.113)–(9.115), curve designated as "Vainshtein *nl*"; the Vainshtein formula averaged over orbital quantum number according to (9.116)–(9.118), curve designated as "Vainshtein *n*"; detailed quantum level-by-level calculations (Behar et al. 1996), curve designated as "quantum." It can be seen that the statistical orbital averaged method compares quite well with the detailed quantum calculations, as does the *l*-averaged Vainshtein approach, in particular, these approaches describe very well the critical low-temperature dielectronic recombination while the Burgess-Mertz approach entirely fails in this region. Figure 9.4 demonstrates also that the difference between the *l*-averaged branching factor and autoionization rate in the statistical approach is rather small; only at very low temperatures, some difference becomes visible.

The great advantage of the statistical model is its generality that also provides an easy means to study scaling laws. Figure 9.5 shows the analysis of the scaling in nuclear charge number Z_n for fixed $kT_e = 100\,\mathrm{eV}$ for the total dielectronic recombination rate obtained from the various approaches discussed in Fig. 9.4. It can be seen that the statistical *l*-averaged approaches as well as the *l*-averaged Vainshtein approach provide a reasonable agreement with the numerical data from complex quantum calculations.

As Figs. 9.4 and 9.5 demonstrate, the l-averaged approaches of the statistical and the Vainshtein approach seem to correspond better with the complex quantum mechanical level-by-level calculations, while the statistical and Vainshtein

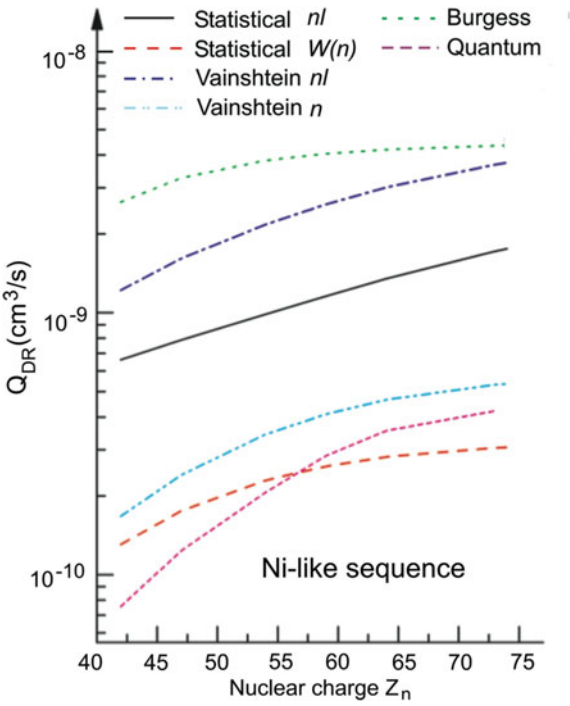

Fig. 9.5 Scaling properties in dependence of nuclear charge Z_n for kT_e = 100 eV for the various statistical approaches compared to quantum level-by-level calculations for the Ni-like sequence $3s^2 3p^6 3d^{10}$

nl-approach provides systematically larger total dielectronic recombination rates. The physical origin of this observation is difficult to explore and has not yet been discussed in the literature. In fact, in the current statistical approaches (Leontyev and Lisitsa 2016) multichannels as depicted by (9.111), (9.112) are not included. Multichannels, however, as have been demonstrated in detail in Sect. 5.6.2.2 may result in a decrease of total dielectronic recombination rate.

Below, we compare the different approaches with detailed quantum mechanical level-by-level calculations of the dielectronic recombination rates. Figure 9.6 shows the total dielectronic recombination rates of Xenon Xe^{26+} and Gold Au^{51+} (Ni-like $3s^2 3p^6 3d^{10}$-configuration into which dielectronic capture proceeds) calculated with the *l*-averaged statistical model from (9.85), (9.93), (9.94) that employs the Thomas–Fermi model of (9.1)–(9.13), the Burgess formula from (9.101)–(9.105) and the quantum level-by-level calculations of Behar et al. (1996).

The statistical model compares quite well (within a factor of two) over a very large temperature interval until very low temperatures while the Burgess approach entirely fails to describe the total dielectronic recombination rate of heavy ions. Similar observations are made for other isoelectronic sequences. Figure 9.7 shows a comparison of the Sr-like and Zn-like dielectronic recombination of tungsten and a comparison with detailed quantum mechanical level-by-level calculations (Wu et al. 2015).

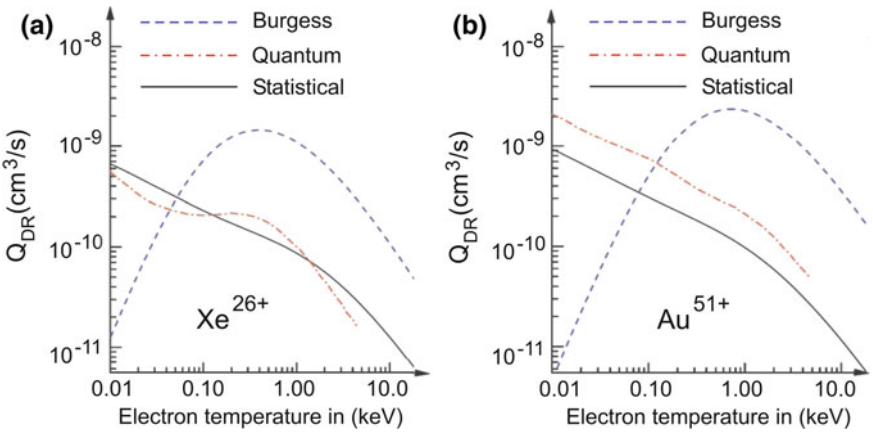

Fig. 9.6 Comparison of the l-averaged statistical approach with the Burgess and quantum level-by-level calculations for the Ni-like sequence $3s^2 3p^6 3d^{10}$ of Xenon Xe^{26+} and Gold Au^{51+}

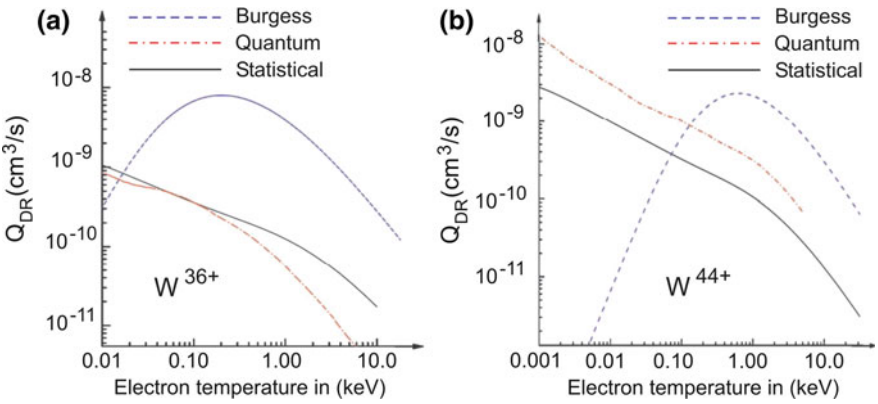

Fig. 9.7 Comparison of the l-averaged statistical approach with the Burgess and quantum level-by-level calculations for the Sr-like sequence $4s^2 4p^6 4d^2$ of Tungsten W^{36+} and the Zn-like sequence $4s^2$ of tungsten W^{44+}

It is particular impressive that the statistical model provides a rather good approximation of the total dielectronic recombination rate in the low-temperature region that is numerically exceedingly difficult to treat by fully quantum level-by-level calculations. Therefore, the statistical model in its simplest version of (9.1)–(9.13), (9.85)–(9.91), (9.92)–(9.95) seems to provide even the possibility to estimate the order of magnitude correctness of very complex quantum level-by-level calculations. Moreover, it should be remembered that currently even the most sophisticated quantum level-by-level calculations (Wu et al. 2015) have been obtained only in the low-density limit (corona approximation) where the

branching factors are entirely determined by radiative and autoionization decay rates while dielectronic capture is proceeding from the respective ground states of the various charge states only. In high-density plasmas, however, collisional depopulation due to electron collisional ionization or collisional transfer to other levels (in particular of high nl-levels) strongly influences on the branching factors (see Sect. 5.6). In addition, excited states are highly populated from which very efficient channels of dielectronic recombination may proceed (Rosmej et al. 2020b). This may entirely change the properties of the total dielectronic recombination because dielectronic capture into excited states can be even more important than corresponding capture to the ground state (Sect. 5.6.3.2). This effect has explicitly been confirmed by high-resolution X-ray spectroscopy of dense laser-produced plasmas where it was shown that dielectronic recombination into excited states might exceed by many orders of magnitude the corresponding dielectronic recombination into ground states (Rosmej et al. 1998; Petitdemange and Rosmej 2013; Rosmej et al. 2020b). As for high-Z elements and open M-, N- and O-shells, excited states might be highly populated even at rather moderate electron densities. Therefore, all current detailed quantum level-by-level calculations to determine the dielectronic recombination have to be considered with care with respect to the particular application. In this respect, the properties and the innovation potential of the statistical model look very advantageous for the determination of the total dielectronic recombination rates for heavy elements.

Finally we note that the inclusion of more levels in the detailed quantum mechanical level-by-level calculations may not necessarily result only in an increase of the dielectronic recombination rate, but can also lead to a decrease as discussed in Sect. 5.6.2.1 and described by (9.111), (9.112). Therefore, at present, the simple above-presented statistical method compares quite well with other available much more complex methods of calculations and has the advantage of generality and ease of application. In addition, there is much room for improvements of the statistical model via improvements of the Thomas–Fermi model (ionization energies, l-quantum number dependence, Vlasov approach instead of the local plasma frequency, etc.).

References

V.A. Astapenko, L.A. Bureyeva, V.S. Lisitsa, Polarization mechanism for bremsstrahlung and radiative recombination in a plasma with heavy ions. Plasma Phys. Rep. **28**, 303 (2002)

V.A. Astapenko, L.A. Bureyeva, V.S. Lisitsa, Plasma models of atom and radiative-collisional processes, in *Reviews of Plasma Physics*, vol. 23, 1, ed. by V.D. Shafranov (Kluwer Academic/Plenum Publishers, New York, 2003); ISBN 0-306-11069-5

C.P. Balance, S.D. Loch, M.S. Pindzola, D.C. Griffin, Dielectronic recombination of W^{35+}. J. Phys. B: At. Mol. Opt. Phys. **43**, 205201 (2010)

P. Beiersdorfer, M.J. May, J.H. Scofield, S.B. Hansen, Atomic physics and ionization balance of high-Z ions: critical ingredients for characterizing and understanding high-temperature plasma. HEDP **8**, 271 (2012)

E. Behar, P. Mandelbaum, J.L. Schwob, A. Bar-Shalom, J. Oreg, W.H. Goldstein, Dielectronic recombination rate coefficients for highly-ionized Ni-like atoms. Phys. Rev. A **54**, 3070 (1996)
I.L. Beigman, L.A. Vainshtein, B.N. Chichkov, Dielectronic recombination. JETP **53**, 490 (1981)
W. Brandt, S. Lundqvist, Atomic oscillations in the statistical approximation. Phys. Rev. **139**, A612 (1965)
A. Burgess, Dielectronic Recombination and the Temperature of the Solar Corona. Astrophys. J. **139**, 776 (1964)
R.G. Cowan, *The Theory of Atomic Structure and Spectra* (California University Press, Berkeley, 1981)
A.V. Demura, M.B. Kadomtsev, V.S. Lisitsa, V.A. Shurygin, Statistical model of radiation losses for heavy ions in plasmas. JETP Lett. **98**, 786 (2013)
A.V. Demura, M.B. Kadomtsev, V.S. Lisitsa, V.A. Shurygin, Universal statistical approach to radiative and collisional processes with multielectron ions in plasmas. HEDP **15**, 49 (2015a)
A.V. Demura, M.B. Kadomtsev, V.S. Lisitsa, V.A. Shurygin, Statistical model of electron impact ionization of multielectron ions. J. Phys. B.: At. Molec. Opt. Phys. **48**, 055701 (2015b)
I.K. Dmitrieva, G.I. Plindov, The improved Thomas-Fermi model: chemical and ionization potentials in atoms. J. Physique **45**, 85 (1984)
S. Dyachkov, P. Leavshov, D. Minakov, Region of validity of the Thomas-Fermi model with corrections. Phys. Plasmas **23**, 112705 (2016)
E. Fermi, Eine statistische Methode zur Bestimmung einiger Eigenschaften des Atoms und ihre Anwendung auf die Theorie des periodischen Systems der Elemente. Zeitschrift für Physik **48**, 73 (1928)
P. Fromy, C. Deutsch, G. Maynard, Thomas-Fermi-like and average atom models for dense and hot matter. Phys. Plasmas **3**, 714 (1996)
P. Gombas, Erweiterung der Statistischen Theroy des Atoms. Zeitschrift für Physik **121**, 523 (1943)
P. Gombas, *Die statistische theorie des Atoms und ihre Anwendungen* (Springer, Wien, 1949)
P. Gombas, Present state of the statistical theory of atoms. Rev. Mod. Phys. **35**, 512 (1963)
I.P. Grant, B.J. McKenzie, P.H. Norrington, D.F. Mayers, N.C. Pyper, An atomic multiconfigurational Dirac-Fock package. Comput. Phys. Commun. **21**, 207 (1980)
G. Kemister, S. Nordholm, A radially restricted Thomas–Fermi theory for atoms. J. Chem. Phys. **76**, 5043 (1982)
V.D. Kirillow, B.A. Trubnikov, S.A. Trushin, Role of impurities in anomalous plasma resistance. Sov. J. Plasma Phys. **1**, 117 (1975)
V.I. Kogan, A.B. Kukushkin, V.S. Lisitsa, Kramers electrodynamics and electron-atomic radiative collisional processes. Phys. Rep. **213**, 1 (1992)
D.S. Leontyev, V.S. Lisitsa, Statistical model of dielectronic recombination of heavy ions in plasmas. Contrib. Plasma Phys. **56**, 846 (2016)
E.H. Lieb, B. Simon, The Thomas–Fermi theory of atoms, molecules and solids. Adv. Math. **23**, 22 (1977)
S.D. Loch, J.A. Ludlow, M.S. Pindzola, A.D. Whiteford, D.C. Griffin, Electron-impact ionization of atomic ions in the W isonuclear sequence. Phys. Rev. A **72**, 052716 (2005)
F. Petitdemange, F.B. Rosmej, Dielectronic satellites and Auger electron heating : irradiation of solids by intense XUV-Free Electron Laser radiation, in *New Trends in Atomic & Molecular Physics—Advanced Technological Applications*, vol. 76, ed. by M. Mohan (Springer 2013), pp. 91–114, ISBN 978-3-642-38166-9
R. Piron, F. Gilleron, Y. Aglitskiy, H.-K. Chung, C.J. Fontes, S.B. Hansen, O. Marchuk, H.A. Scott, E. Stambulchik, Yu. Ralchenko, Review of the 9th NLTE code comparison workshop. HEDP **23**, 38 (2017)
D.E. Post, R.V. Jensen, C.B. Tarter, W.H. Grasverger, W.A. Lokke, Steady-state raditiative coling rates for low-density high-temperature plasmas. ADNDT **20**, 397 (1977)
D. Post, J. Abdallah, R.E.H. Clark, N. Putvinskaya, Calculations of energy losses due to atomic processes in tokamaks with applications to the international thermonuclear experimental reactor divertor. Phys. Plasmas **2**, 2328 (1995)

V.M. Povyshev, A.A. Sadovoy, V.P. Shevelko, G.D. SHirkov, E.G. Vasina, V.V. Vatulin, *Electron-Impact Ionization Cross Sections of H, He, N, O, Ar, Xe, Au, Pb Atoms and their Ions in the Electron Energy Range from the Threshold up to 200 keV*, Preprint JINR E9-2001-148, Dubna 2001

T. Pütterich, R. Neu, R. Dux, A.D. Whiteford, M.G. O'Mullane, H.P. Summers, ASDEX upgrade team, calculation and experimental test of the cooling factor of tungsten. Nuc. Fusion **50**, 025012 (2010)

F.B. Rosmej, A.Ya. Faenov, T.A. Pikuz, F. Flora, P. Di Lazzaro, S. Bollanti, N. Lizi, T. Letardi, A. Reale, L. Palladino, O. Batani, S. Bossi, A. Bornardinello, A. Scafati, L. Reale, Line Formation of High Intensity He_{β}-Rydberg Dielectronic Satellites $1s3lnl'$ in Laser Produced Plasmas. J. Phys. B Lett.: At. Mol. Opt. Phys. **31,** L921 (1998)

F.B. Rosmej, L.A. Vainshtein, V.A. Astapenko, V.S. Lisitsa, Statistical and quantum photoionization cross sections in plasmas: analytical approaches for any configurations including inner shells, Matter and Radiation at Extremes (Review) **5**, 064202 (2020a) open access: https://aip.scitation.org/doi/10.1063/5.0022751

F.B. Rosmej, V.A. Astapenko, V.S. Lisitsa, L.A. Vainshtein, Dielectronic recombination in non-LTE plasmas, Matter and Radiation at Extremes (Review) **5**, 064201 (2020b) open access: https://doi.org/10.1063/5.0014158

H.A. Scott, S.B. Hansen, Advances in NLTE modeling for integrated simulations. HEDP **6**, 39 (2010)

I.I. Sobelman, L.A. Vainshtein, *Excitation of Atomic Spectra* (Alpha Science, 2006); ISBN 978-1842652336

A. Sommerfeld, Integrazione asintotica dell'equazione differentiale di Thomas–Fermi. Rend. R. Accademia dei Lincei **15**, 293 (1932)

M. Stenke, K. Aichele, D. Harthiramani, G. Hofmann, M. Steidl, R. Volpel, E. Salzborn, Electron-impact single-ionization of singly and multiply charged tungsten ions. J. Phys. B: At. Mol. Opt. Phys. **28**, 2711 (1995)

H.P. Summers, *ADAS Users Manual*, JET—IR 06 (Abingdon: JET Joint Undertaking, 1994)

L.A. Vainshtein, V.P. Shevelko, The structure and characteristics of ions in hot plasmas, in *Physika i Technika Spektroscopii* 1986 (in Russian)

A.V. Vinogradov, O.I. Tolstikhin, Plasma approach to the theory of photoabsorption and polarizability of complex atoms. Sov. Phys. JETP **69**, 683 (1989)

Z. Wu, Y. Fu, X. Ma, M. Li, L. Xie, J. Jiang, C. Dong, Electronic impact excitation and dielectronic recombination of highly charged Tungsten ions. ATOMS **3**, 474 (2015)

R. Ying, G. Kalman, Thomas–Fermi model for dense plasmas. Phys. Rev. A **40**, 3927 (1989)